A Superpixel-Based Dual Window RX for Hyperspectral Anomaly Detection

Lang Ren, Liaoying Zhao, and Yulei Wang

***Abstract*— This letter presents a superpixel-based dual window RX (SPDWRX) anomaly detection (AD) algorithm that uses superpixel segmentation (SPS) to adaptively determine the dual window for local RX (LRX) detection, rather than using a fixed dual window. The main premise of SPDWRX is to first divide the hyperspectral image into multiple superpixels and then extend the minimum bounding rectangle to determine the background of each superpixel. Finally, LRX AD is conducted on each pixel in the same superpixel using the same background. Furthermore, a fine SPS method is proposed based on the entropy rate superpixel to quickly obtain uniform superpixels. The experimental results show that the proposed SPDWRX method can significantly improve the detection speed and slightly improve the detection performance, and the modified SPS can further improve the detection performance of SPDWRX.**

***Index Terms*— Anomaly detection (AD), dual window, hyperspectral image (HSI), superpixel segmentation (SPS).**

I. Introduction

HYPERSPECTRAL images (HSIs) are 3-D digital images in both spatial and spectral dimensions. Because the rich spectral information of each pixel in HSI can possess an intrinsic advantage to find and identify the subtle differences of different objects on the ground surface, target detection has been one of the most interesting and fundamental tasks in the HSI [1]. Anomaly detection (AD), known as a special case of target detection, is more practical in actual applications because it aims to find the targets of interest without any prior information [2].

According to [3], AD methods can be divided into statistic methods, such as global Reed–Xiaoli algorithm (GRX) [4], kernel methods, such as support vector data description [5], and other methods [2], [3], [6]. Many currently used statistic AD methods are variants of RX, such as local RX (LRX) [7], weighted-RXD [8], and the spectral-spatial-based local summation method (LSAD) [9], among others. RX detectors that consider pixels which are located in a single window centered on the pixel being tested will lead to a high false alarm rate [3]. To address this issue, a dual-window-based RX (DWRX) [10] and a multiple-window AD (MWAD) [11] were developed to naturally divide the local area into potential target and background regions to purify the background for AD. However, both the DWRX and MWRD sometimes failed to ensure the purity of the background for all pixels because the inner window was a rectangle of a fixed size. Moreover, it is time-consuming to recalculate the covariance matrix and its inverse for each pixel.

In recent years, superpixel segmentation (SPS) has been used for different special tasks in HSI research analysis, such as spectral unmixing [12], band selection [13], and target detection [14]. In this letter, we concentrate on using superpixels to improve the efficiency of RX for HSI.

Two of the most widely used algorithms of superpixel segments in HSI application are based on simple linear iterative clustering (SLIC) [15] and the entropy rate superpixel (ERS) [16]. SLIC is usually modified to operate on all image bands [12], [14], [17], and the ERS is applied to the first three principal components (PCs) after the principal component analysis (PCA) of HSI [13]. One key factor that affects the application effect of superpixels for HSI is the uniformity inside segments [18]. By applying the modified SLIC, the uniformity is always ensured if the segments are small enough, and it is time-consuming. On the contrary, only using the first three PCs, the ERS can quickly get compact and homogeneous superpixels with similar sizes [13], but it fails to ensure the uniformity of each superpixel because only three PCs are used.

This letter attempts to explore a new version of dual-window-based RX on SPS. The three main technical contributions are as follows.

1) In order to quickly obtain uniformed superpixels, superpixels are constructed by fine adjustment based on an optimal spectral similarity metric after PCA-ERS.
2) To improve the background information estimation, a dual window is adaptively determined for each superpixel.
3) To decrease the amount of time consumed, the same background suppression is used for pixels in the same superpixel so that the covariance matrix and its inverse only need to be calculated once for each superpixel.

II. Proposed Method

A. Superpixel Segmentation

The ERS [16] is adopted in this letter for initial SPS. The boundary pixels of the extracted superpixels are then finely

Manuscript received June 1, 2019; revised August 8, 2019; accepted September 8, 2019. Date of publication October 9, 2019; date of current version June 24, 2020. The work of L. Zhao was supported in part by the National Nature Science Foundation of China under Grant 61571170 and in part by the Joint Fund Project of Chinese Ministry of Education under Grant 6141A02022350. The work of Y. Wang was supported in part by the National Nature Science Foundation of China under Grant 61801075 and in part by the Fundamental Research Funds for Central Universities under Grant 3132019218 and Grant 3132019341. *(Corresponding author: Yulei Wang.)*

L. Ren and L. Zhao are with the Department of Computer Science, Hangzhou Dianzi University, Zhejiang 310018, China (e-mail: 1016804570@qq.com; zhaoly@hdu.edu.cn).

Y. Wang is with the Center for Hyperspectral Imaging in Remote Sensing (CHIRS), Information and Technology College, Dalian Maritime University, Dalian 116026, China (e-mail: wangyulei@dmlu.edu.cn).

Color versions of one or more of the figures in this letter are available online at http://ieeexplore.ieee.org.

Digital Object Identifier 10.1109/LGRS.2019.2942949

Algorithm 1 PCA-ERS-FA Superpixel Segmentation

Input: Hyperspectral data set $\mathbf{X} \in \mathbf{R}^{L\times N}$.
Output: Superpixel set $\mathbf{S_A} = \{\mathbf{S}_i\}, i = 1, 2, \ldots, N$.

1: Segmentation base image generation
The principal component analysis is applied to the original HSI to obtain the first principal component and to generate the segmentation base image.
2: Initial superpixel generation by ERS
All pixels in the segmentation base image is divided into N_A disjoint superpixels, which denoted as $\mathbf{S_A} = S_1, S_2, \ldots, S_{N_A}$, by ERS.
3: Fine adjustment of $\mathbf{S_A}$
a) Boundary updates: The candidate superpixels for each boundary pixel in the 8-neighborhood are identified. A correlation function that relates each boundary pixel to the candidate superpixels is calculated. The boundary pixel is assigned to the superpixel corresponding to the minimum correlation value among all superpixel candidates [17].
b) Orphaned pixels connection: Any orphaned pixels that do not belong to the same connected superpixels are eliminated using a connected components algorithm [15].
c) Terminate condition: Steps a) and b) are repeated until either the overall residual error converges to a value less than a certain threshold, or a maximum number of iterations is exceeded.

adjusted to make the superpixels relatively regular and compact. The proposed SPS process is described in Algorithm 1, denoted by PCA-ERS-FA. Only the first PC is used in PCA-ERS-FA rather than three PCs.

The correlation function between the boundary pixels x_i and its jth candidate superpixel in the given algorithm is defined as

$$F_{ij} = wd_{\text{spatial}}(\mathbf{x}_i, \mathbf{s}_j) + (1-w)d_{\text{spectral}}(\mathbf{x}_i, \mathbf{s}_j) \tag{1}$$

where $\mathbf{s}_j$ is the center pixel of the jth candidate superpixel of $\mathbf{x}_i$, and

$$d_{\text{spatial}}(\mathbf{x}_i, \mathbf{s}_j) = 1 - \exp(-\|\mathbf{p}_{\mathbf{x}_i} - \mathbf{p}_{\mathbf{s}_j}\|_2) \tag{2}$$

$$d_{\text{spectral}}(\mathbf{x}_i, \mathbf{s}_j) = \frac{\mathbf{x}_i^T \mathbf{s}_j}{\|\mathbf{x}_i\|\|\mathbf{s}_j\|} \tag{3}$$

where $\mathbf{p}_{\mathbf{x}_i}$ and $\mathbf{p}_{\mathbf{s}_j}$ denote the coordination of pixels $\mathbf{x}_i$ and $\mathbf{s}_j$, respectively.

B. Superpixel-Based Dual Window

Unlike the traditional dual window, in which both windows are rectangular and the sizes of the inner and outer windows are fixed, in the superpixel-based dual window, only the outer window is rectangular, and the size of the outer window is not fixed. Fig. 1 illustrates two samples of the superpixel-based dual window. In each sample, the area in blue is a superpixel, which is just the inner window, and the purple rectangle expresses the outer window. The inner window is notably irregular. The smallest outer rectangle of the superpixel, which is plotted by a yellow dotted line, is used to assist in determining the outer window. As Fig. 1 illustrates, the opposite edges of the two rectangles are spaced at w pixels.

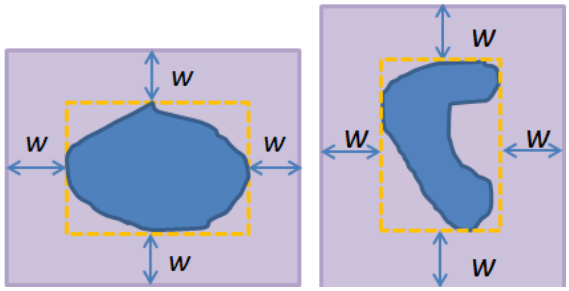

Fig. 1. Samples of the superpixel-based dual window. (a) Sample 1. (b) Sample 2.

C. Superpixel-Based Local RX Algorithm

Let $\mathbf{SP}_i$ denote the pixel set of the ith superpixel of HSI, and the detection value for each pixel in $\mathbf{SP}_i$ is

$$\delta_j\left(\boldsymbol{\mu}_i, \sum\nolimits_i\right) = (\mathbf{x}_j - \boldsymbol{\mu}_i)\sum\nolimits_i^{-1}(\mathbf{x}_j - \boldsymbol{\mu}_i) \tag{4}$$

where $\boldsymbol{\mu}_i$ and $\sum_i$ are the mean vector and the covariance matrix of spatial neighboring pixels located within the superpixel-based dual window of $\mathbf{SP}_i$, respectively, $\mathbf{x}_j$ is the jth pixel in $\mathbf{SP}_i$, $j = 1, 2, \ldots, n_i$, and n_i is the number of pixels in $\mathbf{SP}_i$.

After obtaining superpixels via SPS, the proposed superpixel-based dual window RX (SPDWRX) AD algorithm conducts detection for each pixel in a superpixel-based dual window by the following procedure.

1) *Establish Pixel Ordinal Correspondence:* For each pixel $\mathbf{x}_j$ in a superpixel $\mathbf{SP}_i$, find its corresponding ordinal, which is denoted as I_j in the entire HSI data.
2) *Determine the Superpixel-Based Dual Window:* The outer window of superpixel $\mathbf{SP}_i$ is determined by extending each edge of the smallest outer rectangle of the superpixel by w spaces.
3) *Calculate the Detection Value:* Calculate the detection value of each pixel $\mathbf{x}_j$ in $\mathbf{SP}_i$ with (4), and set $d_{I_j} = \delta_j$.

III. Real Hyperspectral Experiment

To evaluate the performance of the proposed SPDWRX algorithm, our experiment uses three different LRX detection algorithms for comparison. These methods include LRX [7], LSAD [9], and DWRX [10]. Furthermore, the results of SPDWRX using SLIC based on boundary updating (BU) [17], PCA-ERS, and the proposed PCA-ERS-FA are also compared. Considering that the result of RX detection can be prominently improved by subspace projection [9], the inversion of covariance is calculated by SVD in all the algorithms. The experiment uses two real hyperspectral scenes with complete ground truth information of the anomaly target. The area under the receiver operating characteristic (ROC) curve of (P_d, P_f), denoted by area under curve (AUC), is used for evaluation of detection performance. The maximum iterative time of BU in PCA-ERS-FA is set to 5.

A. Experiment on HYDICE Image

A real image scene collected by the hyperspectral digital imagery collection experiments (HYDICEs), shown

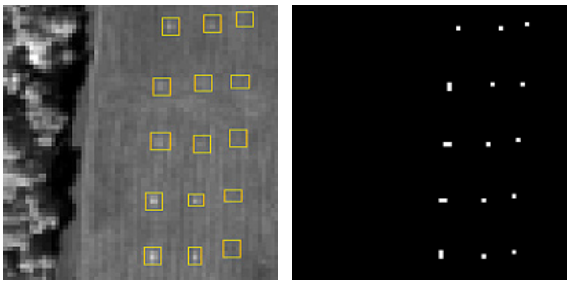

(a) (b)

Fig. 2. (a) HYDICE scene. (b) Ground truth map.

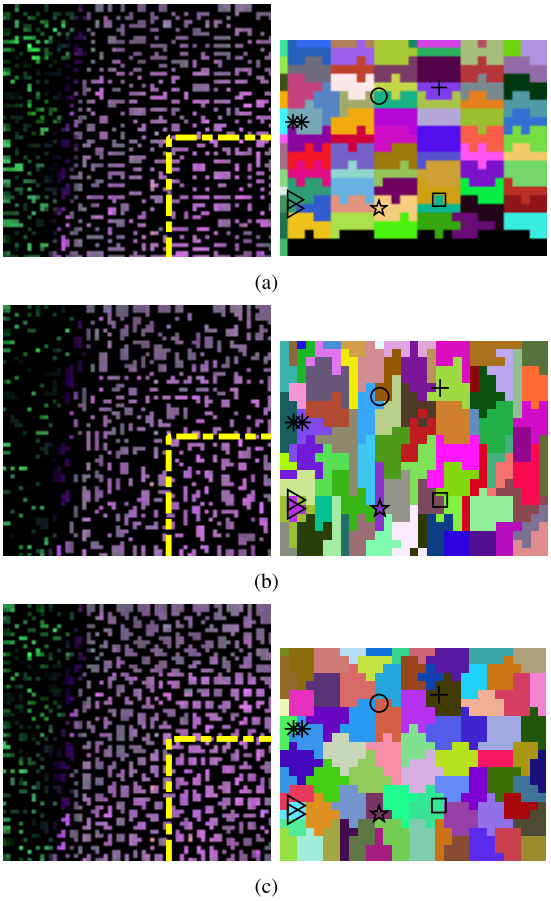

(a) (b) (c)

Fig. 3. Results of SPS. (a) BU. (b) PCA-ERS. (c) PCA-ERS-FA.

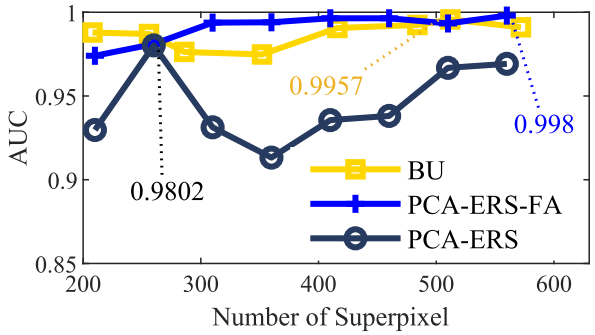

Fig. 4. AUC of SPDWRX with different numbers of superpixels.

in Fig. 2(a), was used for the experiments. It has a total of 169 bands, along with a spatial resolution of 1.56 m and a spectral resolution of 10 nm. Its detailed description can be found in [19]. It has a size of 64 × 64 pixel vectors and 15 man-made panels that can be considered as anomalies in the scene. The ground truth map is provided in Fig. 2(b).

Two experiments are conducted to evaluate our proposed algorithm. The computing time is then discussed.

1) Detection Performance of the SPDWRX With Different Parameters: Fig. 3 shows the results of SPS, wherein each line in the right subimage shows the superpixels of the right bottom area marked by yellow lines in the left subimage, and the object positions are indicated by different markers. Table I shows the AUC of SPDWRX with a different window space w. The number of superpixels is 410, 410, and 416 for PCA-ERS, PCA-ERS-FA, and BU, respectively, as shown in Fig. 3 and Table I. Fig. 3 shows that both BU and PCA-ERS-FA obtained regular superpixels. The superpxiel that contained object marked by star or circle is obviously not well segmented by PCA-ERS, while both are adjusted well by PCA-ERS-FA. It is worth noting that even though the average size of all superpixels is about 10 pixels when the number of superpixel is 410 or 416, most superpixels that contain the objects are less than 10, which is reasonable for HYDICE data with target panels ranging from 2 pixels to 1 pixel. It is worth mentioning that the observations from the experimental results provided in Table I are remarkable.

1) When $w = 3$, the results of SPDWRX using different SPS methods are all obviously better than the results of the other cases. When $w = 4$, BU and PCA-ERS-FA also perform well.
2) The PCA-ERS-FA obtains the largest AUC to 0.9964, which is slightly better than BU, while BU is slightly better than PCA-ERS-FA except for $w = 3$ or 10. The results of PCA-ERS are much worse than the other two methods.

Fig. 4 shows the AUC of SPDWRX by three SPS methods with different numbers of superpixels when the window space is fixed as 3, where the data in different colors are the largest values of AUC for each method. As shown in Fig. 4, as for the largest AUC, all the three methods can obtain a good value and the PCA-ERS-FA is better than BU. On the whole, PCA-ERS is still much worse than the other two methods and PCA-ERS-FA is slightly better than BU in most cases. The AUCs of SPDWRX by PCA-ERS-FA are all near to 1 when the number of superpixels varied from 310 to 600.

Finally, we can conclude from Fig. 3, Table I, and Fig. 4 that 3 or 4 is the relatively proper choice for window space, and the SPDWRX using PCA-ERS-FA is robust to the number of superpixels. In addition, the SPDWRX using PCA-ERS-FA exhibits a significant improvement in detection performance and detection stability compared with using PCA-ERS.

2) Comparison of Different RX Algorithms: Denote the size of the sliding window as $sw \times sw$. By setting sw as [3:2:15], both LRX and LSAD obtain optimal results when $sw = 7$. DWRX obtains the optimal result when $sw_{in} = 3$ and $sw_{out} = 7$. The optimal result of SPDWRX using PCA-ERS-FA is compared with the optimal results of LRX, LSAD, and DWRX. Fig. 5 shows the respective detection maps of the four algorithms. Fig. 6 plots the ROC curves of (P_d, P_f). Table II provides the AUC values for the ROC curves of (P_d, P_f).

TABLE I
DETECTION RESULTS OF SPDWRX WITH DIFFERENT NUMBERS OF SUPERPIXELS (WINDOW SPACE = 3)

segmentation method	window space w							
	3	4	5	6	7	8	9	10
BU	0.9943	0.9923	0.8860	0.7879	0.7373	0.8502	0.9196	0.9122
PCA-ERS	0.9356	0.8977	0.8676	0.7551	0.7510	0.8675	0.9236	0.9105
PCA-ERS-FA	0.9964	0.9880	0.8736	0.7445	0.7253	0.8385	0.9129	0.9126

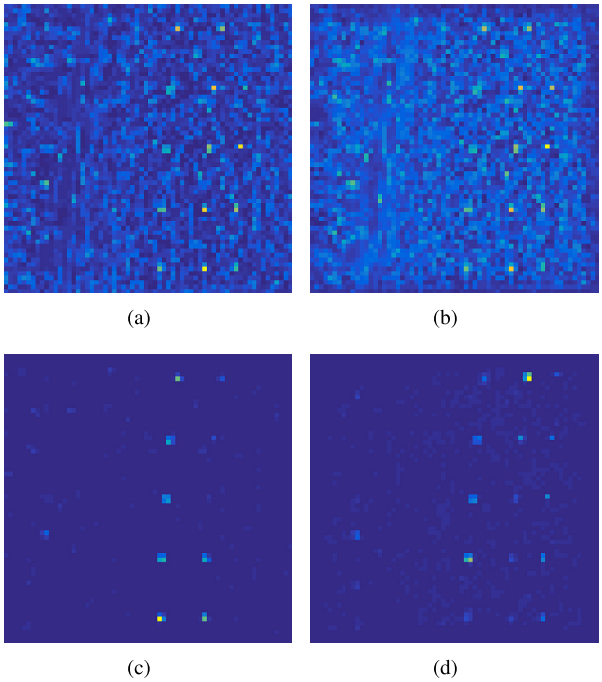

Fig. 5. Detection maps of four LRX algorithms. (a) LRX. (b) LSAD. (c) DWRX. (d) SPDWRX.

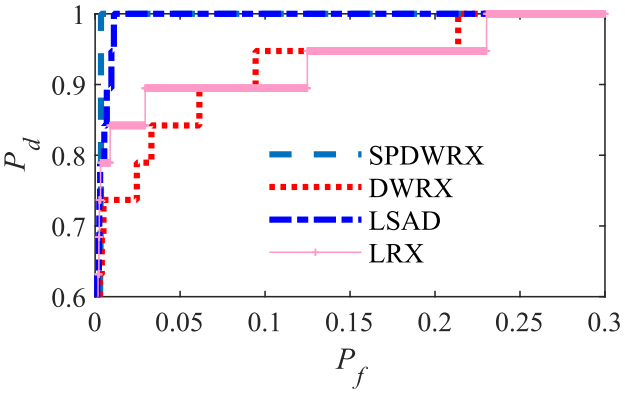

Fig. 6. ROC curve for the detection result of the HYDICE scene.

It is evident from Fig. 5 that SPDWRX exhibits the best background suppression of all the algorithms, as all the object panels are only clearly detected in the respective detection maps of SPDWRX. It is also evident from Fig. 6 and Table II that SPDWRX is slightly better than the other three methods.

TABLE II
AUC VALUES OF THE COMPLETE ROC CURVE OF (P_d, P_f)

method	LRX	LSAD	DWRX	SPDWRX
AUC	0.9785	0.9976	0.9721	0.9980

TABLE III
CPU TIMES OF DIFFERENT ALGORITHMS

method	LRX	LSAD	DWRX	SPDWRX		
				PCA-ERS-FA	PCA-ERS	BU
Time(s)	18.84	20.37	19.23	4.26	2.88	13.71

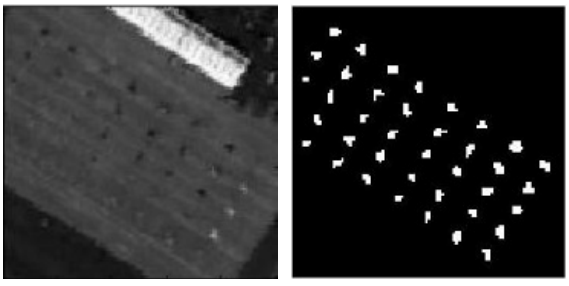

Fig. 7. San Diego airport data. (a) Pseudocolor image. (b) Target map of anomalies in the test region.

3) Computing Time: The computer environments used for the experiments are 64-bit operating systems with Intel i7-7700, a central processing unit (CPU) of 3.60 GHz, and 8 GB of random access memory (RAM). Table III lists the average CPU time of each algorithm after running 5 times, where the number of subpixels for each SPDWRXs is same as shown in Fig. 3, and the time of the SPDWRX includes time for SPS and 1.298 s for RX detection. As provided in Table III, the CPU times of LRX, LSAD, and DWRX are similar, while the total CPU time of each SPDWRX is much less than the other methods. This is primarily because the time required to calculate the covariance matrix and its inverse is largely reduced in SPDWRX, and therefore, the operation efficiency is greatly improved. In addition, BU is more time-consuming than PCA-ERS and PCA-ERS-FA.

B. Experiment on San Diego Airport Data

The experiment uses a subgraph with a size of 100 × 100 cut from San Diego data collected by HYDICEs, and it is

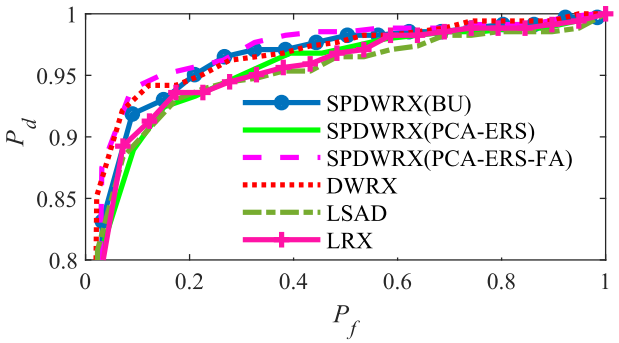

Fig. 8. Comparison of the ROC curves of different algorithms.

TABLE IV
RESULTS OF DIFFERENT ALGORITHMS FOR THE SAN DIEGO IMAGE

method	LRX	LSAD	DWRX	SPDWRX		
				PCA-ERS-FA	PCA-ERS	BU
AUC	0.9511	0.9477	0.9646	0.9675	0.9514	0.9601
Time(s)	53.28	53.57	47.14	9.58	3.04	27.42

shown in Fig. 7(a). Its ground truth is provided in Fig. 7(b). It was acquired by 224 spectral bands with spectral coverage from 0.4 to 2.5 μm. The spatial resolution is 3.5 m, and the spectral resolution is 10 nm. After removing the low-SNR or water vapor absorption (1–6, 33–35, 97, 107–113, 153–166, and 221–224), 189 spectral bands are used in the experiment.

Fig. 8 plots the ROC curves of (P_d, P_f) for the optimal results of the four algorithms. Table IV provides the AUC and CPU time for each method. The parameters are $sw = 13$ for LRX and LSAD, $sw_{in} = 5$ and $sw_{out} = 11$ for DWRX, and $w = 4$ for SPDWRX, and the number of superpixels is 350, 350, and 357 for PCA-ERS, PCA-ERS-FA, and BU, respectively.

It can be seen from Fig. 8 and Table IV that SPDWRX (PCA-ERS-FA) obtains the best result. Compared with SPDWRX (PCA-ERS), the AUC is increased by 0.016. Both SPDWRXs by ERS run much faster than LRX and LSAD. The time of SPDWRX by BU is almost half the time of LRX or LSAD.

IV. CONCLUSION

This letter develops a new dual RX AD method based on SPS, as well as a modified SPS method based on PCA-ERS. In contrast to three typical LRX algorithms, the advantages of the new RX detection approach include a small increase in detection performance and a large increase in speed. The proposed SPS method can further improve detection performance by taking slightly more time. In the future work, the performance of SPDWRX is to be verified by using other SPS methods, such as uniformity-based SPS [18]. In addition, the applicability of the algorithm to scenes with substantial different sizes anomalies or anomalies close together need to be further verified.

ACKNOWLEDGMENT

The authors would like to thank all the developers of the superpixel segmentation methods who kindly offered their code. The statements made herein are the sole responsibility of the authors.

REFERENCES

[1] N. M. Nasrabadi, "Hyperspectral target detection: An overview of current and future challenges," *IEEE Signal Process. Mag.*, vol. 31, no. 1, pp. 34–44, Jan. 2014.
[2] L. Zhu, G. Wen, S. Qiu, and X. Zhang, "Improving hyperspectral anomaly detection with a simple weighting strategy," *IEEE Geosci. Remote Sens. Lett.*, vol. 16, no. 1, pp. 95–99, Jan. 2019.
[3] M. Vafadar and H. Ghassemian, "Hyperspectral anomaly detection using combined similarity criteria," *IEEE J. Sel. Topics Appl. Earth Observ. Remote Sens.*, vol. 11, no. 11, pp. 4076–4085, Nov. 2018.
[4] I. S. Reed and X. Yu, "Adaptive multiple-band CFAR detection of an optical pattern with unknown spectral distribution," *IEEE Trans. Acoust., Speech Signal Process.*, vol. 38, no. 10, pp. 1760–1770, Oct. 1990.
[5] S. Khazai, S. Homayouni, A. Safari, and B. Mojaradi, "Anomaly detection in hyperspectral images based on an adaptive support vector method," *IEEE Geosci. Remote Sens. Lett.*, vol. 8, no. 4, pp. 646–650, Jul. 2011.
[6] L. Wei and D. Qian, "Collaborative representation for hyperspectral anomaly detection," *IEEE Trans. Geosci. Remote Sens.*, vol. 53, no. 3, pp. 1463–1474, Mar. 2015.
[7] J. M. Molero, E. M. Garzón, I. García, and A. Plaza, "Analysis and optimizations of global and local versions of the rx algorithm for anomaly detection in hyperspectral data," , vol. 6, no. 2, pp. 801–814, 2013.
[8] Q. Guo, B. Zhang, Q. Ran, L. Gao, J. Li, and A. Plaza, "Weighted-RXD and linear filter-based RXD: Improving background statistics estimation for anomaly detection in hyperspectral imagery," *IEEE J. Sel. Topics Appl. Earth Observ. Remote Sens.*, vol. 7, no. 6, pp. 2351–2366, Jun. 2014.
[9] B. Du, R. Zhao, and L. Zhang, "A spectral-spatial based local summation anomaly detection method for hyperspectral images," *Signal Process.*, vol. 124, pp. 115–131, Jul. 2016.
[10] H. Kwon, S. Z. Der, and N. M. Nasrabadi, "Adaptive anomaly detection using subspace separation for hyperspectral imagery," *Opt. Eng.*, vol. 42, no. 11, pp. 3342–3351, Nov. 2003.
[11] W. M. Liu and C. I. Chang, "Multiple-window anomaly detection for hyperspectral imagery," *IEEE J. Sel. Topics Appl. Earth Observ. Remote Sens.*, vol. 6, no. 2, pp. 644–658, Apr. 2013.
[12] Z. Li, J. Chen, and S. Rahardja, "Superpixel construction for hyperspectral unmixing," in *Proc. 26th Eur. Signal Process. Conf. (EUSIPCO)*, Sep. 2018, pp. 647–651.
[13] C. Yang, L. Bruzzone, H. Zhao, Y. Tan, and R. Guan, "Superpixel-based unsupervised band selection for classification of hyperspectral images," *IEEE Trans. Geosci. Remote Sens.*, vol. 56, no. 12, pp. 7230–7245, Dec. 2018.
[14] Y. Liang, P. P. Markopoulos, and E. S. Saber, "Subpixel target detection in hyperspectral images with local matched filtering in SLIC superpixels," in *Proc. 8th Workshop Hyperspectral Image Signal Process., Evol. Remote Sens. (WHISPERS)*, Aug. 2016, pp. 1–5.
[15] R. Achanta, A. Shaji, K. Smith, A. Lucchi, P. Fua, and S. Süsstrunk, "SLIC superpixels compared to state-of-the-art superpixel methods," *IEEE Trans. Pattern Anal. Mach. Intell.*, vol. 34, no. 11, pp. 2274–2282, Nov. 2012.
[16] M.-Y. Liu, O. Tuzel, S. Ramalingam, and R. Chellappa, "Entropy rate superpixel segmentation," in *Proc. CVPR*, Jun. 2011, pp. 2097–2104.
[17] A. Çahşkan, A. Koz, and A. A. Alatan, "Hyperspectral superpixel extraction using boundary updates based on optimal spectral similarity metric," in *Proc. IEEE Int. Geosci. Remote Sens. Symp. (IGARSS)*, Jul. 2015, pp. 1020–1023.
[18] A. M. Saranathan and M. Parente, "Uniformity-based superpixel segmentation of hyperspectral images," *IEEE Trans. Geosci. Remote Sens.*, vol. 54, no. 3, pp. 1419–1430, Mar. 2016.
[19] C.-I. Chang, *Hyperspectral Data Processing: Algorithm Design and Analysis*. Hoboken, NJ, USA: Wiley, 2013.